Original Article

MOLECULAR METABOLISM

Pyruvate and uridine rescue the metabolic profile of OXPHOS dysfunction

Isabelle Adant [1,2], Matthew Bird [1,2,3], Bram Decru [1,2], Petra Windmolders [1], Marie Wallays [1], Peter de Witte [4], Daisy Rymen [5], Peter Witters [5], Pieter Vermeersch [3,6,8], David Cassiman [1,5,*,8], Bart Ghesquière [2,7,8,]**

ABSTRACT

Introduction: Primary mitochondrial diseases (PMD) are a large, heterogeneous group of genetic disorders affecting mitochondrial function, mostly by disrupting the oxidative phosphorylation (OXPHOS) system. Understanding the cellular metabolic re-wiring occurring in PMD is crucial for the development of novel diagnostic tools and treatments, as PMD are often complex to diagnose and most of them currently have no effective therapy.

Objectives: To characterize the cellular metabolic consequences of OXPHOS dysfunction and based on the metabolic signature, to design new diagnostic and therapeutic strategies.

Methods: *In vitro* assays were performed in skin-derived fibroblasts obtained from patients with diverse PMD and validated in pharmacological models of OXPHOS dysfunction. Proliferation was assessed using the Incucyte technology. Steady-state glucose and glutamine tracing studies were performed with LC-MS quantification of cellular metabolites. The therapeutic potential of nutritional supplements was evaluated by assessing their effect on proliferation and on the metabolomics profile. Successful therapies were then tested in a *in vivo* lethal rotenone model in zebrafish.

Results: OXPHOS dysfunction has a unique metabolic signature linked to an NAD+/NADH imbalance including depletion of TCA intermediates and aspartate, and increased levels of glycerol-3-phosphate. Supplementation with pyruvate and uridine fully rescues this altered metabolic profile and the subsequent proliferation deficit. Additionally, in zebrafish, the same nutritional treatment increases the survival after rotenone exposure.

Conclusions: Our findings reinforce the importance of the NAD+/NADH imbalance following OXPHOS dysfunction in PMD and open the door to new diagnostic and therapeutic tools for PMD.

Keywords Primary mitochondrial disease; OXPHOS; Aspartic acid; Treatment; Pyruvate and uridine

1. INTRODUCTION

Primary mitochondrial diseases (PMD) are a group of disorders caused by pathogenic variants in genes that are vital for normal mitochondrial function [1]. Their estimated prevalence is at least 1 in 5,000 individuals [1,2]. PMD form a heterogeneous group of pathologies due to their highly diverse clinical presentation in which the involvement of any organ at any age with any severity can be seen, and complex modes of genetic transmission with inherited or de novo pathogenic variants in both nuclear genome (autosomal recessive, autosomal dominant or X-linked inheritance patterns) and mitochondrial DNA (mtDNA, passed down through the maternal lineage). As mammalian cells contain hundreds of copies of their mitochondrial genome per cell, the percentage of mtDNA carrying a pathogenic mutation may vary. This phenomenon, known as heteroplasmy, can further complicate the clinical picture since possible variation in heteroplasmy can occur in variably affected tissues [1]. Due to this heterogeneity, diagnosing PMD poses a challenge which often results in a long "diagnostic odyssey" for the patients [3].

The biochemical basis of PMD is impaired mitochondrial function which typically manifests itself as a disrupted activity of the oxidative

[1]Laboratory of Hepatology, Department of Chronic Diseases, Metabolism and Ageing, KU Leuven, Leuven, 3000, Belgium [2]Metabolomics Expertise Center, Center for Cancer Biology, CCB-VIB, VIB, Leuven, 3000, Belgium [3]Clinical Department of Laboratory Medicine, University Hospitals Leuven, Leuven, 3000, Belgium [4]Laboratory for Molecular Biodiscovery, Department of Pharmaceutical and Pharmacological Sciences, KU Leuven, Leuven, 3000, Belgium [5]Metabolic Centre, University Hospitals Leuven, Leuven, 3000, Belgium [6]Department of Cardiovascular Sciences, KU Leuven, Leuven, 3000, Belgium [7]Metabolomics Expertise Center, Department of Oncology, KU Leuven, Leuven, 3000, Belgium

[8] These authors contributed equally to this work.

*Corresponding author. Laboratory of Hepatology, Department of Chronic Diseases, Metabolism and Ageing, KU Leuven, Leuven, 3000, Belgium. E-mail: david.cassiman@kuleuven.be (D. Cassiman).

**Corresponding author. Metabolomics Expertise Center, Center for Cancer Biology, CCB-VIB, VIB, Leuven, 3000, Belgium. E-mail: bart.ghesquiere@kuleuven.be (B. Ghesquière).

Received April 11, 2022 • Revision received May 31, 2022 • Accepted June 23, 2022 • Available online 27 June 2022

https://doi.org/10.1016/j.molmet.2022.101537

Abbreviations

aKG	alpha-ketoglutarate
BrdU	5-bromo-2′-deoxyuridine
dpf	days post fertilization
DHODH	dihydroorotate dehydrogenase
glycerol-3-P	glycerol-3-phosphate
IEM	inborn errors of metabolism
LDH	Lactate Dehydrogenase
(C) I—V	mitochondrial complexes
$\Delta\Psi m$	mitochondrial membrane potentials
NAD	nicotinamide dinucleotide
OAA	oxaloacetic acid
OXPHOS	oxidative phosphorylation system
PARP	poly ADP ribose polymerase
PMD	primary mitochondrial diseases
PDH	pyruvate dehydrogenase
SD	standard deviation
TMRM	tetramethyl rhodamine methyl ester
TCA	tricarboxylic acid cycle

phosphorylation system (OXPHOS, mitochondrial complexes (C) I—V). Historically, OXPHOS deficiency has largely been studied in isolation as the dysfunction of one or multiple complex(es), without considering the impact thereof on interconnected pathways [4,5,6]. OXPHOS is not only required for energy generation, it is also the determining factor in key biochemical processes such as the maintenance of the cellular redox equilibrium by preserving a high NAD+/NADH balance [7]. Since numerous metabolic reactions rely on the electron exchange with the NAD+/NADH couple, OXPHOS dysfunction can be expected to have an indirect but important impact on numerous cellular metabolic reactions relying on those cofactors [8]. The characterization of cellular metabolic re-wiring that occurs in PMD patients would therefore serve as a stepping stone enabling the development of (personalized) treatments. This mind shift is critical, as to date, therapeutic options are not available for the vast majority of PMD [6,9].

To understand how metabolic pathways are affected, and more specifically how the connectivity of pathways is affected, we applied tracer metabolomics onto a diverse set of models of OXPHOS diseases. Tracer metabolomics provides insights into the connectivity of the active cellular metabolic network by tracing non-radioactive isotopically labelled atoms of labelled nutrients (tracers) into metabolic routes that rely on these labelled nutrients [10]. Consequently, this method not only delivers information about the abundance of the cellular metabolites, but also provides fractional contribution data of the labelled nutrient. Isotopic labelling of metabolites (isotopologues) can be further exploited to derive metabolic flux information. Therefore, it provides a read-out that is closely related to the actual functioning of the cellular metabolic activity. Here, we applied tracing of U—^{13}C-labeled glucose and U—^{13}C-glutamine to determine the metabolic profile of OXPHOS dysfunction in genetic and pharmacological models of PMD [11—13]. Our results reveal a distinct and universal signature of OXPHOS deficiency with as main feature the depletion of aspartic acid. Moreover, our work led to the design of a treatment strategy that is able to restore, both *in vitro* and *in vivo,* the metabolic deregulation induced by OXPHOS deficiency via correction of the NAD+/NADH balance.

2. MATERIALS, SUBJECTS AND METHODS

2.1. Ethics and patient derived cell lines

The analyses of fibroblasts were approved by the ethical committee of the University Hospitals of Leuven under application number S60206 (retrospective metabolic analysis of archived fibroblasts) and S58977 (prospective assessment of mitochondrial function in fibroblasts). Informed consent was obtained from the patients or their legal guardian(s).

Fibroblasts from individuals with different genetically confirmed causes of PMD and control fibroblasts cell lines obtained from healthy individuals were retrospectively recruited from the UZ Leuven fibroblast databank.

2.2. Cell culture

Fibroblasts from patients with PMD and healthy controls were maintained in DMEM medium with 5.5 mM glucose (closest approximation to physiological glycemia) and 2 mM glutamine supplemented with 10% foetal bovine serum at 37 °C with 5% CO_2 in a humidified incubator. Unless otherwise specified, experiments were performed in pyruvate free medium. Cells were not allowed to grow further than passage 15. Cells were screened for Mycoplasma infection (Westburg). OXPHOS dysfunction was pharmacologically induced in fibroblasts from healthy donors by applying rotenone at a concentration of 30 nM, 100 nM and 200 nM, antimycin A at a concentration of 1 μM and azide at a concentration of 500 μM. Rotenone (100 mM), antimycin A (5 mM) azide (4M) first stock solutions were prepared in ethanol.

2.3. Reagents

All reagents were from Sigma unless otherwise specified. DMEM medium was purchased from ThermoFisher. Stable isotopes (tracers) were purchased from Cambridge Isotope Laboratories.

2.4. Stable isotope tracer studies

Fibroblasts were plated at 4,500 to 5,500 cells/cm^2/0.15 mL of DMEM (ThermoFisher) with 5.5 mM Glucose, 2 mM Glutamine and no pyruvate in 6-well plates. The exact plating number was determined to obtain a confluency of 60%—90% 72 h after seeding. After 24 h, cells, and empty wells (background), were washed once in PBS, and then refilled with 1.5 mL DMEM containing either 5.5 mM U—^{13}C Glucose and 2 mM U—^{12}C Glutamine; 5.5 mM U—^{12}C Glucose and 2 mM U—^{13}C Glutamine; or 5.5 mM U—^{12}C Glucose and 2 mM U—^{12}C Glutamine. At 72 h, samples were collected by collecting the media and harvesting the cells on ice. Once the media removed, wells were washed once in ice cold saline solution (9 g/L NaCl), after which the cells were scraped in 200 μL of ice-cold extraction buffer (80% methanol (Merck), 2 μM d27 myristic acid) and transferred to a 1.5 mL tube and stored overnight at −80 °C. The cellular debris was then pelleted (20,000 g, 15 min, 4 °C), and the supernatant transferred to a new vial and again centrifuged (20,000 g, 15 min, 4 °C). The supernatant was set aside for analysis by mass-spectrometry (see further). Protein content of the cell pellet was determined by BCA assay (ThermoFisher Scientific) after dissolution of the pellet in 100 μL of 200 mM NaOH (20 min, 95 °C). For the mass-spectrometry analysis, 30 μL of sample were then separated on an ion pairing liquid chromatography column, and the metabolites resolved on a Q Exactive™ Hybrid Quadrupole-Orbitrap™ Mass Spectrometer in negative ion mode with ESI settings (40 sheet gas flow rate, auxiliary gas flow rate 10, spray voltage of 4.8 kV, S-lens RF level of 60 and the capillary

temperature at 300 °C). A full scan (resolution set at 140,000 at 200 *m/z*, AGC at 3e6, 512 ms ion fill time and 70–1,050 *m/z* scan range) was applied.
Metabolites were finally quantified according to their elution time and *m/z* ratios using the open-source analysis platform EL-MAVEN. Coupled processing of the data in POLLY™ integrated correction of naturally occurring carbon isotopes. Metabolite abundances were normalized to protein content. Abundances were expressed relative to the abundance of the control(s) analysed in the same experiment.

2.5. Oxygraphy

Oxygraphy was performed as described previously [11] using the Oxygraph O2K from Oroboros instruments accordingly to previously published resources with a technical n of $\geq$3 [11,14]. Briefly, fibroblasts were harvested by trypsinisation from a T175 flask at a density of 80%, washed in PBS (phosphate buffered saline) and resuspended in Miro5 buffer to 20 million cells/mL. Two million cells (100 μL) were injected per oxygraph chamber. Subsequently, the following compounds were injected to the final concentration of: digitonin, (Merck) 7.5 μg/mL as determined by a digitonin titration; pyruvate, 5 mM; malate, 0.5 mM; ADP (Calbiochem), 1 mM; glutamate, 10 mM; succinate, 10 mM; carbonyl cyanide m-chlorophenyl hydrazone (CCCP), Δ 0.5 μM till maximum respiration reached; rotenone, 75 nM; glycerophosphate, 10 mM; antimycin A, 250 nM; ascorbate sodium salt (Merck), 2 mM; N,N,N′,N'-Tetramethyl-p-phenylenediamine dihydrochloride (TMPD), 0.5 mM; sodium azide, 200 mM. Oxygen saturation was maintained at $\geq$ 40 μM throughout the experiment, and at $\geq$ 180 μM before the measurement of isolated complex IV (CIV) activity.

2.6. Proliferation studies

The proliferation rates of the fibroblasts were assayed using the Incucyte ZOOM™ live cell imaging system (Sartorius). Briefly, fibroblasts were plated at 5,000 cells/cm^2/0.33 mL of DMEM with 5.5 mM Glucose, 2 mM Glutamine and no pyruvate in 96-well plates. Medium was refreshed daily to compensate for the non-humidified atmosphere of the Incucyte. Real-time proliferation was assessed from hour 22 to hour 72 after seeding using the ZOOM™ software. Cell counts were obtained by applying Vybrant® DyeCycle™ Green (Life Technologies) at 0.25 μM at 72 h and read on the green channel of the Incucyte after 1–2 h staining. The images were again processed by the Incucyte coupled ZOOM™ software.
Mitochondrial membrane potentials ($\Delta\Psi$m) were assessed by applying tetramethyl rhodamine methyl ester (TMRM) at a concentration of 40 nM at 72 h and fluorescence intensities were determined after 2 h using a FluostarOmega spectrophotometer (BMG Labtech, fluorescence intensity mode, excitation 544nm/emission 590 nm). TMRM values were expressed relative to cell counts by Vybrant® DyeCycle™ Green.
5-bromo-2′-deoxyuridine (BrdU) assays (Roche) were performed according to the manufacturer's notice. Briefly, BrdU was added to the 96 wells at hour 48 at a total concentration of 100 μM. At 72 h, medium was removed, and the cells were dried for 15min at 60 °C. The plate was stored at 4 °C for max one week. The assay itself was performed by fixating, then incubating the wells with the anti-BrdU-antibody for 90 min followed by 3 washes with PBS. Finally, 50 μL of the substrate solution was added to the wells and absorbances were read after 7 min (FluostarOmega spectrophotometer (BMG Labtech), absorbance mode, 450 nm).
TMRM values and BrdU values were expressed relative to the untreated cells plated in the same experiment.
All proliferation experiments were plated in triplicates and at least 3 repeats (2 for BrdU) were performed per cell line. Those repeats were averaged to retain one value per cell line for statistics.

2.7. In vitro treatment trials

To test different experimental treatments, DMEM with 5.5 mM Glucose, 2 mM Glutamine, 10% FBS and no pyruvate was supplemented at plating with chosen nutrients to a total concentration of: citrate, 1 mM; Dimethyl L-Aspartate (Tokyo Chemical Industry), 150 μM; Fructose, 500 μM; niacin, 1 mM; pyruvate, 1 mM; sorbitol, 500 μM; uridine, 200 μM; adenine, 200 μM; guanine, 200 μM; thymidine, 200 μM. Ketogenic diet was mimicked by lowering glucose concentration to 3.5 mM and adding acetoacetate at 1.5 mM. Results were compared with cells plated in parallel without supplementation.
The size of the OXPHOS deficient group in which the efficacy of treatment was tested by tracer metabolomics was previously determined by a power calculation aiming at normalisation of aspartic acid values (Fisher exact test to reach 80% power to detect a difference between untreated and treated cell lines; calculated sample size n = 9).

2.8. Rotenone zebrafish model

The wild-type AB strain was obtained from the Zebrafish International Resource Centre. Adult zebrafish were kept at 28.5 °C, on a 14/10 h light/dark cycle under standard aquaculture conditions, as described previously [15]. Fertilized eggs were collected via natural spawning. Embryos and larvae were kept in embryo medium (1.5 mM HEPES, pH 7.6, 17.4 mM NaCl, 0.21 mM KCl, 0.12 mM MgSO4 and 0.18 mM Ca(NO3)2), and maintained on a 14/10 h light/dark cycle in an incubator at 28.5 °C. For the described experiments, larvae at 7 days post fertilization (dpf) were used. All zebrafish experiments were approved by the Ethics Committee of the University of Leuven and by the Belgian Federal Department of Public Health, Food Safety & Environment (LA1210199). All experiments were conducted in accordance with the Act of 15 January 2015 on the protection of animals used for scientific and educational purposes, Directive 2010/63/EU of the European Parliament and of the Council of 22 September 2010 on the protection of animals used for scientific purposes.
Pharmacological OXPHOS inhibition was obtained by treating the larvae on 7 dpf with 150 or 200 nM rotenone for 6 h [13,16]. Rotenone first stock solutions (100 mM) were prepared in ethanol, second stock solutions (100 μM) in DMSO. Control larvae were treated with equal amount of DMSO (vehicle). Survival (defined as beating heart) was assessed hourly after application of the toxin. Pyruvate and uridine treatment was applied simultaneously with the rotenone on 7 dpf.
Based on previously published data [13] showing that in the control group all animals (100%) displayed a normal brain whereas in case of rotenone-induced OXPHOS dysfunction, the prevalence of normal brains was reduced to 20% (SD 10%), we estimated that a delta (Δ) of 30% between the rotenone-treated and the rescued group would be sufficiently large to show a beneficial effect of the uridine/pyruvate treatment. A power calculation (Fisher exact test) provided a need for 44 animals per group to reach 80% power to detect a difference between 20% and 50%.

2.9. Statistics

Error bars describe +/− standard deviation (SD). Technical replicates were averaged for statistical analysis. Normality testing was performed by Shapiro–Wilk tests. Disease groups were compared using an ANOVA with Dunnett's post-hoc with comparison of all pairs with correction of

the P-values for multiple testing. Effect of treatment was assessed using two-sided paired student T-tests comparing no treatment with a treatment. Zebrafish survival curves were compared using the Mantel—Cox. Statistical analyses were performed using GraphPad Prism (Version 9.3.1 (350), 2021). *P*-values < 0.05 are reported.

3. RESULTS

3.1. Patient cohort

A diverse set of fibroblasts consisting of 17 cell lines obtained from individuals with different genetically confirmed causes of OXPHOS dysfunction, 15 control fibroblasts cell lines obtained from healthy individuals and 3 fibroblasts cell lines from individuals with a pyruvate dehydrogenase (PDH) deficiency was recruited from the UZ Leuven fibroblast databank. The group with OXPHOS dysfunction included cell lines with an isolated complex deficiency (CI: 8 cell lines, CIV: 2 cell lines, CV: 2 cell lines) and combined deficiency (5 cell lines, all being mitochondrial translation machinery defects). Seventy-six percent (13/17) defects were encoded for by nuclear genes, 24% (4/17) by mtDNA. The phenotypic diagnosis of OXPHOS dysfunction in these fibroblast cell lines was previously characterised through enzymology and oxygraphy [11]. We included the PDH cell lines as a comparison group with non-OXPHOS related mitochondrial dysfunction. A complete list of the cell lines and the affected genes is provided in Table 1.

3.2. OXPHOS deficiency leads to a proliferation deficit

OXPHOS dysfunction impairs mitochondrial function in general and thus disrupts ATP production and NAD + regeneration from NADH, thereby impacting a wide variety of metabolic pathways [8,17,18]. We hypothesized that, amongst other cell functions, OXPHOS dysfunction would impair cellular proliferation [19,20]. To verify this, we designed a proliferation assay for skin-derived fibroblasts using the Incucyte® technology. The doubling time, based on confluency changes over a 48-hours period, was calculated for the diverse set of fibroblasts described in section 3.1.

As expected, we noticed an increase in the doubling time of the OXPHOS deficient cell lines with a mean doubling time of 26 h vs. 20 h in the control fibroblasts (Figure 1A). The slower proliferation of OXPHOS deficient cells was validated by a complementary lower absolute nucleus count with the Vybrant® DyeCycle™ Green 72 h after plating of 1500 cells/well (mean cell count of controls versus OXPHOS deficiency 6148 vs. 5384; $p = 0.5$; Fig. S2A).

3.3. OXPHOS dysfunction is linked to a distinct metabolic profile

To understand the proliferation defect in OXPHOS dysfunction, we decided to investigate the role of metabolic pathways and whether these would reveal a metabolic signature for OXPHOS deficiency. For this, we performed a series of tracer metabolomics screens on the aforementioned set of fibroblasts. Given the critical role of OXPHOS in the generation of energy and redox factors, we decided to focus on the central carbon-related metabolic pathways (glycolysis, pentose phosphate pathway and Krebs cycle), and branching pathways of synthesis and/or degradation of amino acids and nucleotides. With fully labelled glucose (U—^{13}C glucose) and glutamine (U—^{13}C glutamine) we gained comprehensive insight into the activity and connectivity of the central carbon-related pathways (Figure 1B). Practically, fibroblasts were incubated for 48 h with the selected tracers to ensure a steady state, an equilibrated condition with stable delivery of the tracing molecules and the inflow of non-labelled nutrients.

In the tracer experiments, cells with OXPHOS dysfunction indeed exhibited distinct metabolic features. Overall, there were increased levels of glycolytic intermediates (Figure 1B and C), and lower amounts

Table 1 — Overview of skin-derived fibroblast cell lines obtained from healthy controls and patients with a genetic diagnosis of PMD.

System	Sub-system	Pseudonym	Affected gene (^{M} mtDNA)	NCBI reference sequence	Pathogenic variants (^{S} splice site mutation)	Heteroplasmy levels (if mtDNA variant)
Control	Control	C1-5; C9; C16-18; C20-25	/			
OXPHOS	CI	P2736	*NDUFS2*	NM_004550	Homozygous c.1336G > A (p.Asp446Asn)	
		P2737	*NDUFS1*	NM_005006	c.1057G > C (p.Ala353Pro), c.420+2T > C (^{S})	
		P45	*TMEM126B*	NM_018480	c.401delA (p.Arg134Ilefs*2), c.635G > T (p.Gly212Val)	
		P2937	*MT—ND1* ^{M}	NC_012920	m.3928G > C (p.Val208Leu)	85%
		P33	*MT—ND1* ^{M}	NC_012920	m.3481G > A (p.Glu59Lys)	50%
		P30	*ACAD9*	NM_014049	c.976G > C (p.Ala326Thr), c.1552C > T (p.Arg518Cys)	
		P2902	*ACAD9*	NM_014049	c.1687C > G, (p.His563Asp), c.380G > A (p.Arg127Gln)	
		P2943	*NUBPL*	NM_025152	c.693+1G > A (^{S}), c.351G > A (p.Met117Ile)	
	CIV	P52	*SURF1*	NM_003172	c.312_321delinsAT (p.Pro104_Leu105insTer), c.544_545delinsCA (p.Val182His)	
		P55	*SURF1*	NM_003172	c.845_856del (p.Ser282Cysfs*), c.870insA (p.Lys291Ter)	
	CV	P2264	*MT-ATP6* ^{M}	NC_012920	m.8993T > G (p.Leu156Arg)	ND (fibroblasts); >85% in leukocytes and muscle
		P2911	*ATP5F1D*	NM_001687	Homozygous c.245C > T (p.Pro82Leu)	
	Combined	P50	*MT-TD* ^{M}	NC_012920	m.7526A > G	2—3%
		P43	*MRPL44*	NM_022915	Homozygous c.467T>G, (p.Leu156Arg)	
		P2912	*MRPL44*	NM_022915	c.481_484delinsTC (p.Thr161Serfs*2), c.467T>G (p.Leu156Arg)	
		P2909	*CARS*	NM_005548	c.123dupC (p.Lys42Glyfs*5), c.683C>T (p.Pro228Leu)	
		P34	*EARS2*	NM_133451	c.286G>A (p.Gln96Lys), c.500G>A (p.Cys167Tyr)	
PDH		P31	*PDHA1*	NM_000284	c.523G > A (p.Ala175Thr), WT	
		P2130	*PDHA1*	NM_000284	c.904C > T (p.Arg302Cys), WT	
		P2940	*PDHA1*	NM_000284	Hemizygous NA (p.Asn164Ser)	

PMD: primary mitochondrial disease, OXPHOS: oxidative phosphorylation system, C: Control, P: Patient, CI: Complex I, CIV: Complex IV, CV: Complex V, PDH: Pyruvate Dehydrogenase NDUFS:NADH Ubiquinone Oxidoreductase Core Subunit, TMEM: transmembrane protein, ND: Complex I subunit; ACAD: Acyl-Coenzyme A Dehydrogenase; NUBPL: Nucleotide Binding Protein Like, SURF: Surfeit Locus Protein, ATP5F1D: ATP Synthase F1 Subunit Delta, MT-TD: Mitochondrially Encoded TRNA-Asp (GAU/C), MRPL: Mitochondrial Ribosomal Protein L, CARS: Cysteinyl-TRNA Synthetase, EARS: Glutamyl-TRNA Synthetase; NA: details not available.

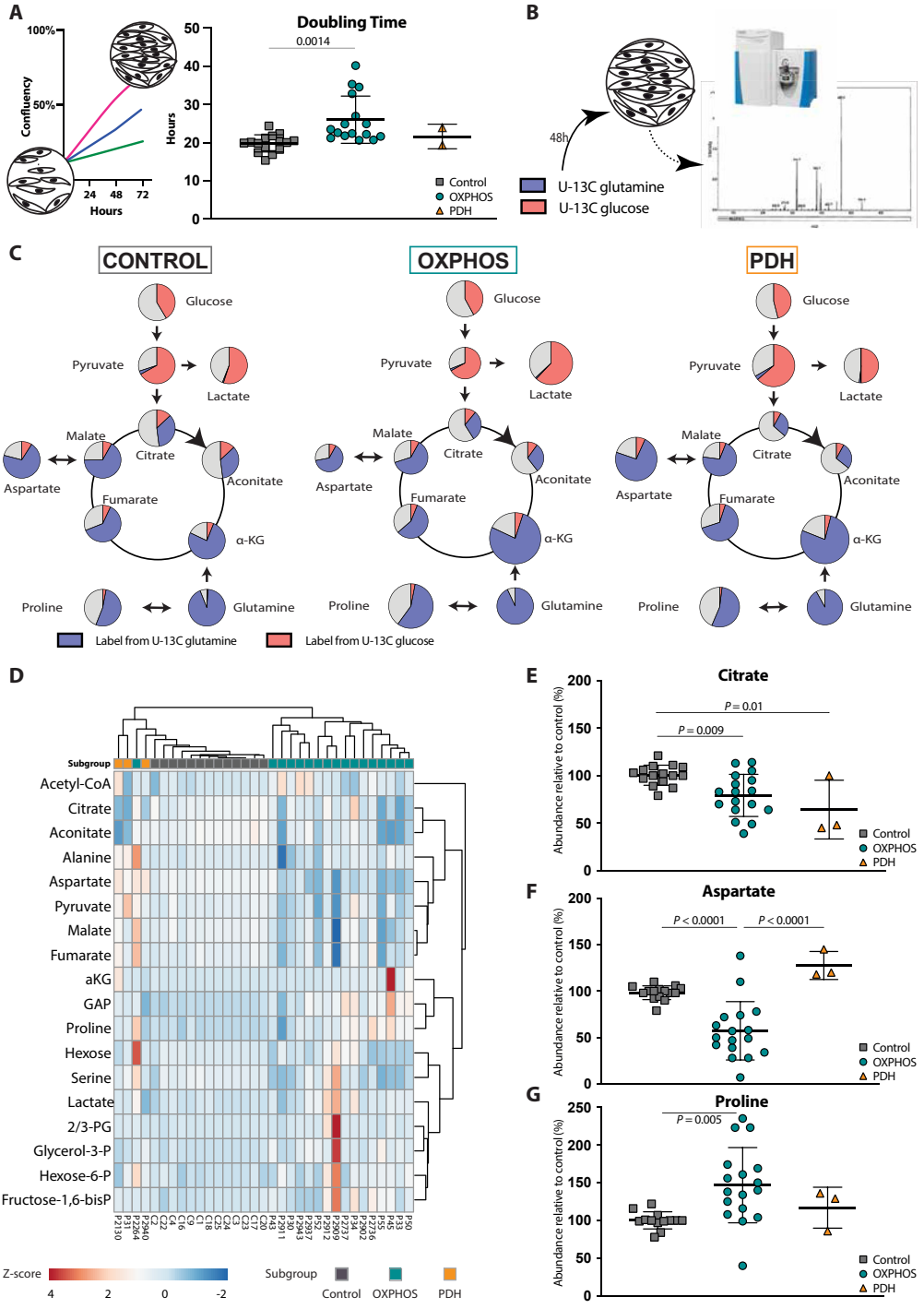

Figure 1: Metabolic profile of mitochondrial disease A Design of the fibroblast proliferation assays based on 72-hours Incucyte® proliferation experiments. Doubling time was calculated over a 48-hour period starting 24 h after plating (control (n = 15), OXPHOS deficient (n = 17) and PDH deficient (n = 3) fibroblast cell lines; technical replicates >3 per cell line). **B** Design of the tracer-based metabolomics studies with cultures with U−^{13}C glucose or U−^{13}C glutamine. **C** A simplified map of glycolysis and TCA cycle is depicted. The area of the circles represents the relative abundance of the metabolite compared to average control. Pink, blue and grey colour represent the fractional labelling coming from U−^{13}C glucose, U−^{13}C glutamine or other sources, respectively. **D** Heatmap displaying the changes in metabolite relative abundances of glycolysis, TCA and linked amino acids relative to controls in the different fibroblast cell lines. The colour scale (blue to red) corresponds to the z-score value of the relative abundance of the metabolite. Grouping of the different cell lines into disease subgroups is annotated with different colours: OXPHOS deficiency; PDH deficiency and controls. Full description of the genetic deficiency per cell line is described in Table 1. **E** The relative abundances of citrate, **F** aspartate and **G** proline in control, OXPHOS deficient and PDH deficient fibroblasts. Tracer metabolomics in control (n = 15), OXPHOS deficient (n = 17) and PDH deficient (n = 3) fibroblast cell lines (technical replicates 1−3 per cell line). Abundances normalized for protein content (BCA) and to the average of the controls per experiment. Statistics: one-way ANOVA with post-hoc Dunnett's T3 multiple comparison tests, and the error bars are +/−SD. αKG: alpha-ketoglutarate; CoA: coenzyme A; DHAP: dihydroxyacetone phosphate; Fructose-1,6-bisP: fructose-1,6-bisphosphate; GAP: glyceraldehyde-3-phosphate; Glycerol-3-P: Glycerol-3-phosphate; Hexose-6-P: Hexose-6-phosphate; OXPHOS: oxidative phosphorylation system; PDH: pyruvate dehydrogenase; PEP: phosphoenolpyruvate; TCA: tricarboxylic acid; 2/3-PG: 3-phosphoglycerate.

of tricarboxylic acid cycle (TCA) intermediates (Figure 1C). Based on this metabolic profile, it was possible to distinguish the control, OXPHOS deficiency and PDH deficient cell lines (Figure 1D) by the following features: (1) lactate/pyruvate ratio, (2) levels of TCA cycle intermediates, (3) aspartic acid and proline levels, and (4) glycerol-phosphate levels.

As expected, changes in the intracellular lactate/pyruvate ratio were observed in OXPHOS deficiency revealing a significantly higher lactate and lower pyruvate abundance (Figure 3A—B) causing a significant increase of the ratio (1.8-fold; $p = 0.014$; Fig. S2G). This was further corroborated by an increased lactate excretion in the growth medium of the cells (Figure 3C). As well, the label incorporation from U—^{13}C glucose into fully labelled (m3 isotopologue) lactate further reinforced this finding (Figure 3D). Of interest, fibroblasts with PDH deficiency had a decreased lactate/pyruvate ratio compared to controls. The main reason for this was the accumulation of pyruvate (Figure 3A—B; ratio is 0.65-fold compared to ratio in controls; $p = 0.12$; Fig. S2G).

When we focused on the TCA intermediates, we observed a drop in the abundances from the PMD cellular extracts (PDH and OXPHOS) with the mean abundance of citrate (Figure 1E), aconitate, fumarate and malate ranging between 77 and 87% of their abundances found in controls (non-significant decrease except for cis-aconitate; $p < 0.001$; Figure 1D,F, G). The trend in the decrease of TCA intermediates was also accompanied by a decreased labelling derived from glucose (Figure 2C) evidenced by a drop of the representative m2 isotopologue in the TCA intermediates from U—^{13}C glucose (Figure 2A,C, D). In parallel, the TCA anaplerosis of U—^{13}C glutamine via alpha-ketoglutarate (aKG) was similar to controls (Figure 3J). Interestingly,

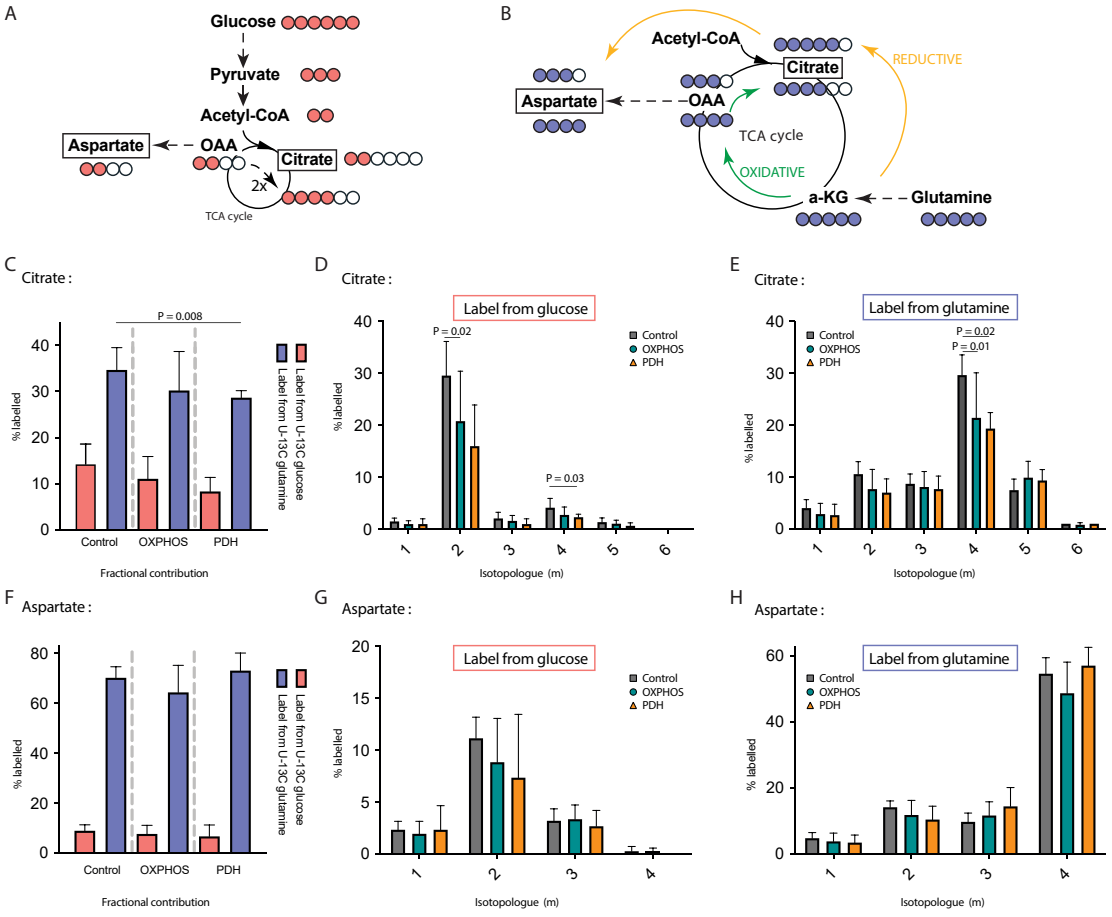

Figure 2: TCA alterations in OXPHOS dysfunction A Schematic representation of anaplerotic glucose flux into the TCA cycle metabolites with cataplerotic efflux and conversion into aspartic acid. The circles represent the number of carbons, with pink filled circles the number of labelled carbons coming from fully labelled U—^{13}C glucose. **B** Schematic representation of anaplerotic glutamine flux into the TCA cycle metabolites with cataplerotic efflux and conversion into aspartic acid. The circles represent the number of carbons, with blue filled circles the number of labelled carbons coming from fully labelled glutamine. **C** Fractional carbon labelling data of citrate in control, OXPHOS deficient and PDH deficient fibroblasts cell lines cultured with U—^{13}C glucose or U—^{13}C glutamine. **D** Comparison of the 6 isotopologues of citrate in control, OXPHOS deficient and PDH deficient fibroblasts cell lines cultured with U—^{13}C glucose or **E** U—^{13}C glutamine. **F** Fractional carbon labelling data of aspartate in control, OXPHOS deficient and PDH deficient fibroblasts cell lines cultured with U—^{13}C glucose or U—^{13}C glutamine**. G** Comparison of the 4 isotopologues of aspartate in control, OXPHOS deficient and PDH deficient fibroblasts cell lines cultured with U—^{13}C glucose or **H** U—^{13}C glutamine. Tracer metabolomics in control (n = 15), OXPHOS deficient (n = 17) and PDH deficient (n = 3) fibroblast cell lines (technical replicates 1—3 per cell line). Abundances normalized for protein content (BCA) and to the average of the controls per experiment. Statistics: one-way ANOVA with post-hoc Dunnett's T3 multiple comparison tests, and the error bars are +/—SD. a-KG: alpha-ketoglutarate; CoA: coenzyme A; OAA: oxaloacetate; OXPHOS: oxidative phosphorylation system; PDH: pyruvate dehydrogenase; TCA: tricarboxylic acid.

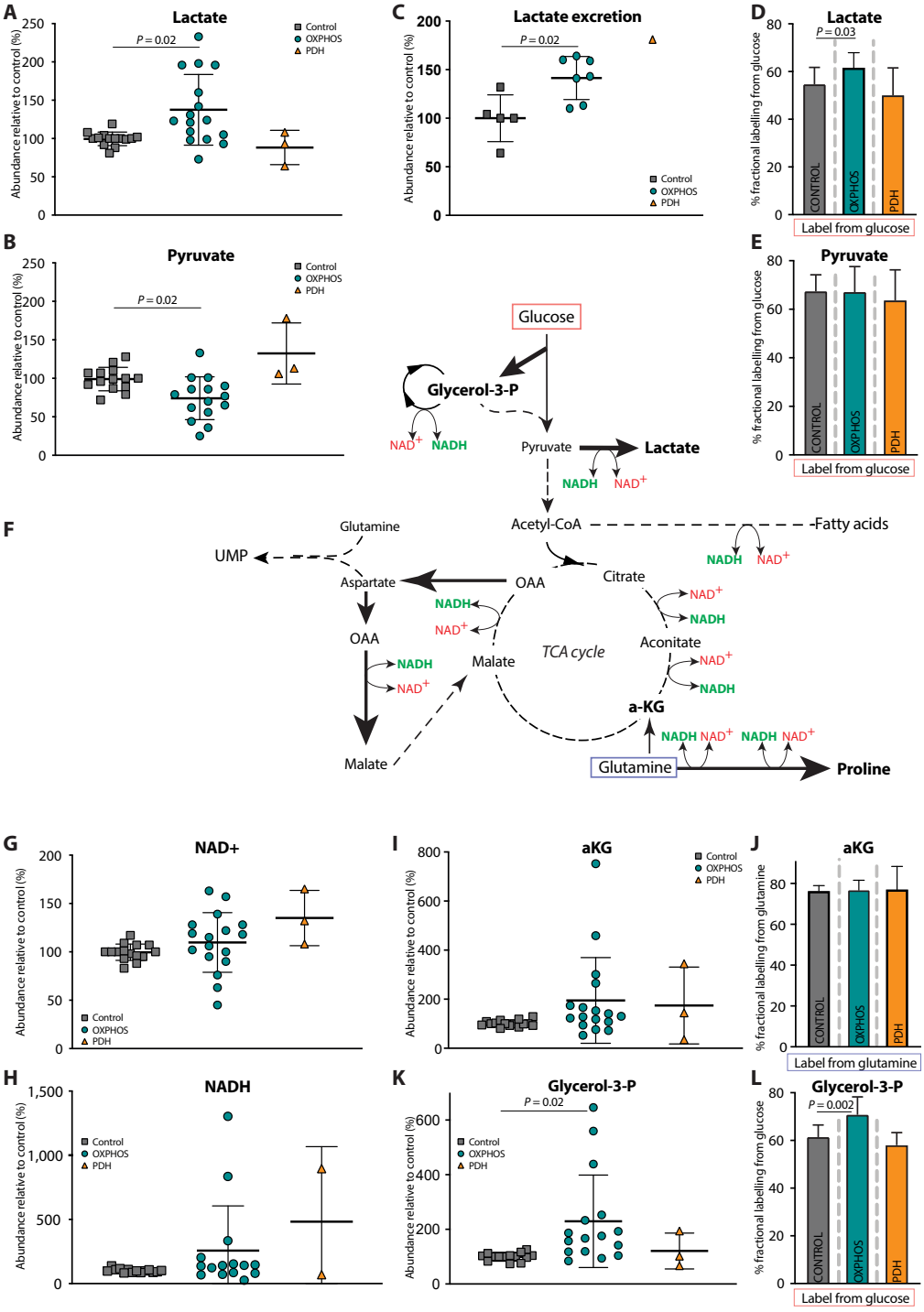

Figure 3: Metabolic profile of OXPHOS dysfunction is linked to NAD+/NADH imbalance. **A** The relative intracellular abundances of lactate and **B** pyruvate in control, OXPHOS deficient and PDH deficient fibroblasts. **C** The relative excretion of lactate in medium in control (n = 5), OXPHOS deficient (n = 7) and PDH deficient (n = 1) fibroblast. **D** Fractional labelling in lactate and **E** pyruvate coming from U−^{13}C glucose in control, OXPHOS deficient and PDH deficient fibroblasts. **F** Schematic representation of the central carbon metabolic reactions using NAD+/NADH as cofactors. Thickness of the arrows and the size of the metabolites indicate the magnitude of alteration in OXPHOS deficient fibroblasts compared to control. **G** The relative intracellular abundances of NAD+ and **H** NADH in control, OXPHOS deficient and PDH deficient fibroblasts. **I** The relative intracellular abundance of aKG and **J** the fractional labelling in aKG coming from U−^{13}C glutamine in control, OXPHOS deficient and PDH deficient fibroblasts. **K** The relative intracellular abundance of Glycerol-3-P and **L** the fractional labelling in Glycerol-3-P coming from U−C glucose in control, OXPHOS deficient and PDH deficient fibroblasts. Unless otherwise specified, tracer metabolomics in control (n = 15), OXPHOS deficient (n = 17) and PDH deficient (n = 3) fibroblast cell lines (technical replicates 1−3 per cell line). Abundances normalized for protein content (BCA) and to the average of the controls per experiment. Statistics: one-way ANOVA with post-hoc Dunnett's T3 multiple comparison tests, and the error bars are +/−SD. a-KG: alpha-ketoglutarate; CoA: coenzyme A; Glycerol-3-P: glycerol-3-phosphate; OAA: oxaloacetate; OXPHOS: oxidative phosphorylation system; PDH: pyruvate dehydrogenase; TCA: tricarboxylic acid.

our tracer data revealed a shift from oxidative cycling (m4 isotopologue of citrate) into reductive cycling (m5 isotopologue of citrate) in both disease groups (Figure 2E) with a lower total fractional labelling derived from glutamine into citrate (Figure 2C).

Investigating the amino acids, we noticed a marked decrease of intracellular aspartic acid triggered by OXPHOS deficiency (Figure 1F). This drop was accompanied by labelling changes in a similar trend to aforementioned changes of TCA intermediates, being a tendency to find less m2 isotopologue derived from U—^{13}C glucose, and more reductive and less oxidative cycling of U—^{13}C glutamine than seen in controls (Figure 2F—H). On the contrary, an increased abundance of aspartic acid was noted In the PDH group (Figure 1F). Increased intracellular proline levels were also observed in OXPHOS deficiency (Figure 1G).

Lastly, a significant elevation of glycerol-3-phosphate (glycerol-3-P) was measured in the OXPHOS deficient cell lines (Figure 3K) with a markedly increased contribution derived from glucose U—^{13}C carbons (Figure 3L).

A detailed overview of the relative abundances of aspartate, proline, lactate and glycerol-3P per OXPHOS deficient cell line is provided in Figure 3A, C, E, G.

3.4. Metabolic profile of OXPHOS dysfunction is linked to NAD+/NADH imbalance

Based on the findings described above, we surmised that the observed metabolic changes related to a disturbed NAD+/NADH balance [8] as a common denominator. Indeed, one of the key tasks of the OXPHOS system is to regenerate NAD+ from NADH (as performed by complex I, NADH:ubiquinone oxidoreductase) [4]. When the OXPHOS system is impaired, the oxidation of NADH is expected to be impaired leading to an accumulation of NADH. In the cellular extracts from the OXPHOS deficient fibroblast cell lines, we observed a tendency towards increased NADH leading to a decreased NAD+/NADH ratio compared to controls (Figure 3G—H).

As a result of this imbalance, several metabolic reactions relying on the NAD+/NADH ratio could be altered (Figure 3F). Consequently, several mechanisms will be activated to restore this critical (im)balance. First, as shown above, the pyruvate/lactate imbalance impacts Lactate Dehydrogenase (LDH), the enzyme driving pyruvate reduction into lactate with regeneration of NAD+ [1,8]. As mentioned previously, we found an increased lactate/pyruvate ratio in our metabolomics data with an increased labelling from U—^{13}C glucose into lactate further supporting the increased activity of LDH to correct the NAD+/NADH balance (Figure 3A—E; Fig. S2G). Second, our data suggests an expanded use of the glycerol-3-P shuttle, as evidenced by the increased glycerol-3-P levels (Figure 3K—L). This shuttle forms a potential mechanism to by-pass CI by transferring reduced equivalents from glycolysis into glycerol-3-P dehydrogenase which oxidizes 1 NADH in the process. Additionally, as our results also showed an increased proline production (Figure 1G), the biosynthesis pathway of proline starting from glutamine provides the cell with 2 NAD + equivalents.

The lower availability of NAD+ and pyruvate are known influencers of pyruvate dehydrogenase activity leading to decreased production of acetyl-CoA and thus lower flux from glucose into the TCA cycle and hence a lower abundance of citrate [21]. The decreased abundance of citrate combined with aKG within normal range leads to an increased aKG/citrate balance (ratio is 2.5x increased in OXPHOS compared to controls; $p = 0.06$; Fig. S2H). This is a known predictor of increased reductive cycling of the TCA cycle [22]: the higher the ratio, the more reductive cycling of glutamine, as we indeed also found.

3.5. Aspartic acid depletion is a hallmark of OXPHOS dysfunction

Aspartic acid production stems from the TCA cycle by AST (aspartic acid transaminase, also known as GOT, glutamate oxaloacetate transaminase) producing aspartic acid and aKG from oxaloacetic acid (OAA) and glutamate. The majority of cells rely on this reaction for aspartic acid availability as the tissue expression of a plasma membrane transporter for aspartic acid is restricted, for example expressed in the central nervous system, epithelial and adipose tissue, but not in the liver [19,20,23]. The diminished aspartic acid abundance in OXPHOS deficient cells (Fig. 1F) could be the result of a lower AST catalysed synthesis. This would be driven by a lower abundance of TCA intermediates such as oxaloacetate, in combination with a disturbed malate-aspartate shuttle function following NAD+/NADH imbalance and an increased use of cytosolic aspartic acid by malate dehydrogenase to oxidize NADH (Figure 3F). Aspartic acid is a key amino acid for several critical cellular metabolic pathways such as the urea cycle and nucleotide biosynthesis, and its depletion is expected to have detrimental consequences for the cell [19,20]. Obviously, fibroblasts are not an ideal model to study the urea cycle and our results did not show differences in nucleotide pools between healthy control fibroblasts and PMD fibroblasts. Nevertheless, as described earlier, cells with OXPHOS deficiency displayed a proliferation deficit compared to control fibroblasts, which amongst others, could be related to nucleotide biosynthesis deficits.

3.6. Rotenone-induced metabolic changes mimic severe OXPHOS dysfunction

To validate our results in well-established experimental models of mitochondrial dysfunction, we investigated whether pharmacological inhibitors of the OXPHOS such as the CI inhibitor rotenone, the CIII inhibitor antimycin A, or the CIV inhibitor azide, could induce disturbances in control fibroblasts that would mimic the profile of genetic OXPHOS dysfunction [12]. For instance, from a concentration of 30 nM of rotenone, control fibroblasts exhibit features of CI dysfunction by oxygraphy, as depicted by an increased Q-point ratio [11] (Fig. S4). Therefore, we titrated the concentrations of those compounds in the growth medium of healthy fibroblasts to induce a slower proliferation rate, matching the proliferation rate of OXPHOS deficient cell lines as described earlier (Figure 1A). Indeed, at 200 nM rotenone, 1 μM antimycin A or 500 μM of azide, the doubling time of control fibroblasts rose to the values found in the PMD group with OXPHOS deficiency (Figure 5A—B). This lower proliferation was confirmed by lower cell counts at 72 h (Vybrant® DyeCycle™ Green; Fig. S2F) and by lower integration of 5-bromo-2′-deoxyuridine (BrdU; Fig. S2B). A low (30 nM) and high (200 nM) dose of rotenone concentration were subsequently selected for further experiments in control fibroblasts, in a steady-state tracer metabolomics experiment with U—^{13}C glucose and U—^{13}C glutamine to investigate the metabolic profile triggered by rotenone. The main characteristics of the rotenone profile are the same as those seen in the genetic OXPHOS dysfunction including (1) a dose-related marked depletion of aspartate, pyruvate, and TCA intermediates, (2) a dose-related reduced flux of glucose into the TCA and reduced oxidative cycling of glutamine in the TCA and (3) dose-related increased NADH and glycerol-3-P (Figure 5C—I).

3.7. The proliferation deficit is relieved by supplementation with pyruvate and uridine

Following the identification of the metabolic changes observed in OXPHOS deficiency, we investigated which change was instrumental in causing the proliferation deficit that we initially observed. We

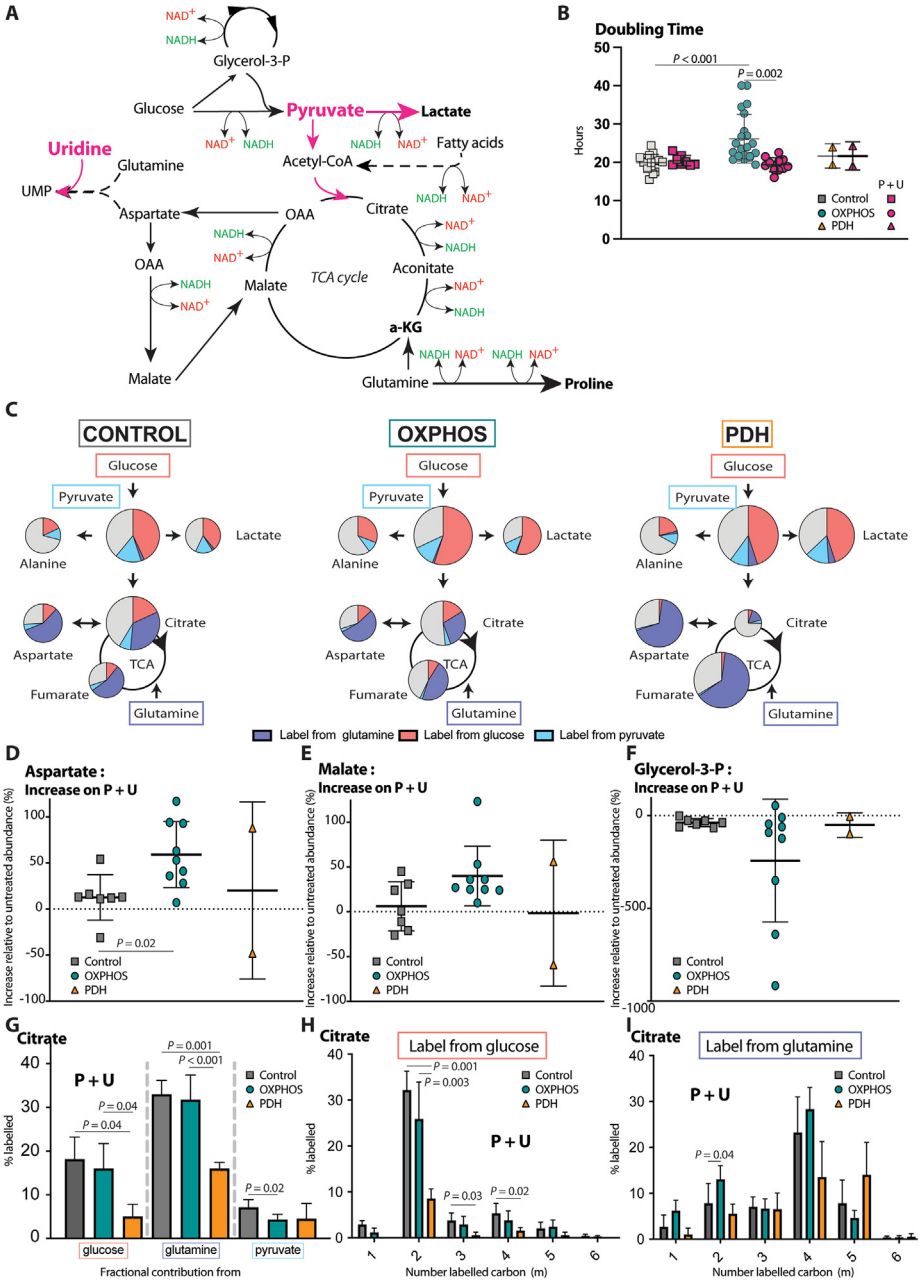

Figure 4: 1 mM Pyruvate and 200 μM uridine supplementation rescues the metabolic consequences of OXPHOS dysfunction in fibroblasts. A Schematic representation of the central carbon metabolic reactions using NAD+/NADH as cofactors depicting the treatment mechanisms of pyruvate + uridine. Thickness of the arrows and the size of the metabolites indicate the magnitude of alteration in OXPHOS deficient fibroblasts compared to control. **B** Effect of pyruvate + uridine supplementation on the doubling time, based on 72-hours Incucyte® proliferation experiments (Controls n = 8; OXPHOS deficient n = 11; PDH deficient n = 2; technical replicates >3 per cell line) with calculation of doubling time over a 48-hour period starting 24 h after plating. **C** Tracer metabolomics faith of glucose, glutamine and pyruvate in 1 mM pyruvate and 200 μM uridine supplemented cultures of controls, OXPHOS and PDH deficient fibroblasts with U−^{13}C glucose, U−^{13}C glutamine or U−^{13}C pyruvate. A simplified map of glycolysis and TCA cycle is depicted. The area of the circles represents the relative abundance of the metabolite compared to average control. Pink, dark blue, light blue and grey colour represent the fractional labelling coming from glucose, glutamine, pyruvate or other sources, respectively. **D** The relative change in abundances of aspartate, **E** malate and **F** glycerol-3-phosphate in controls, OXPHOS deficient and PDH deficient fibroblasts upon supplementation with 1 mM pyruvate and 200 μM uridine. **G** Fractional carbon labelling of citrate in control, OXPHOS deficient and PDH deficient fibroblasts cell lines supplemented with 1 mM pyruvate and 200 μM uridine, cultured with U−^{13}C glucose, U−^{13}C glutamine or U−^{13}C pyruvate. **H** Comparison of the 6 isotopologues of citrate in control, OXPHOS deficient and PDH deficient fibroblasts cell lines cultured with U−^{13}C glucose or **I** U−^{13}C glutamine after supplementation with 1 mM pyruvate and 200 μM uridine. Tracer metabolomics in control (n = 8), OXPHOS deficient (n = 9) and PDH deficient (n = 2) fibroblast cell lines (technical replicates 1−3 per cell line). Abundances normalized for protein content (BCA) and to the average of the controls per experiment. Statistics: one-way ANOVA with post-hoc Dunnett's T3 multiple comparison tests, effect of treatment was assessed using paired student T-tests comparing no treatment with a treatment and the error bars are +/−SD. αKG: alpha-ketoglutarate; dpf: days post fertilisation; Glycerol-3-P: Glycerol-3-phosphate; OXPHOS: oxidative phosphorylation system; PDH: pyruvate dehydrogenase; P + U: 1 mM pyruvate +200 μM uridine.

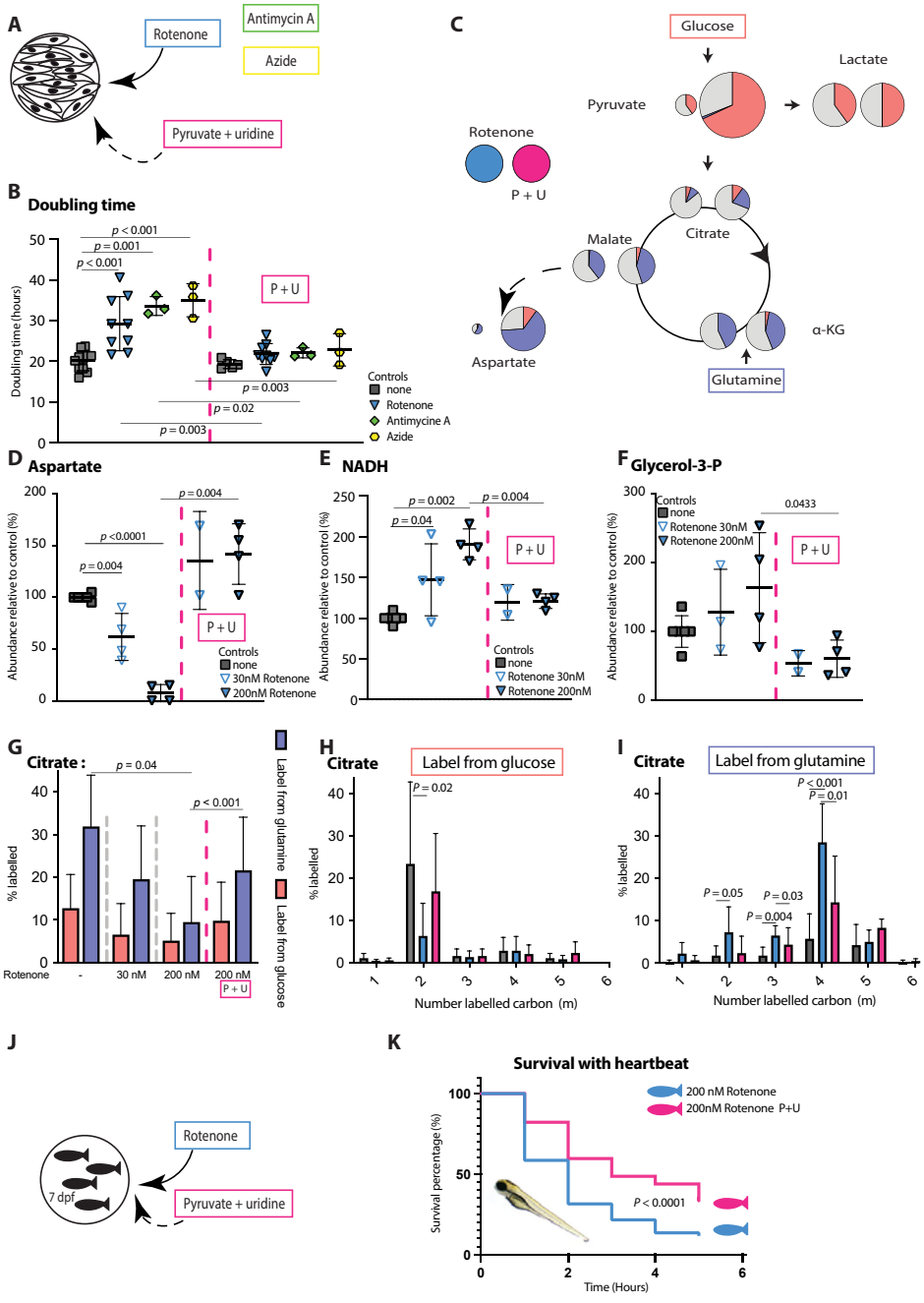

Figure 5: Combination of pyruvate and uridine rescues rotenone induced OXPHOS dysfunction in fibroblasts and zebrafish models A Rotenone, antimycin A and azide model of OXPHOS dysfunction in control fibroblast, treated by 1 mM pyruvate and 200 μM uridine. **B** Doubling time of control fibroblasts exposed to with 200 nM rotenone (n. = 9), 1 μM antimycin A (n = 3) and 500 μM azide (n = 3) with the effect of pyruvate + uridine supplementation thereon. Doubling time based on 72-hours Incucyte® proliferation experiments (technical replicates >3 per cell line) with calculation over a 48-hour period starting 24 h after plating. **C** Tracer based metabolomics results from fibroblasts cultured with U−^{13}C glucose or U−$^{13}C_5$ glutamine. A simplified map of glycolysis and TCA cycle is depicted. The area of the circles represents the relative abundance of the metabolite compared to average control. Pink, blue and grey colour represent the fractional labelling coming from glucose, glutamine or other sources, respectively. A comparison of rotenone OXPHOS dysfunction (left) with and without pyruvate-uridine treatment (right) is shown. **D** The relative abundances of aspartate, **E** NADH and **F** glycerol-3-phosphate in controls, 30 nM and200 nM rotenone induced OXPHOS dysfunction and pyruvate-uridine treatment in the 30 nM and200 nM rotenone groups. **G** Fractional carbon contribution of citrate in control, 30 nM and 200 nM rotenone induced OXPHOS dysfunction and pyruvate-uridine treatment in the 200 nM rotenone group. Fibroblasts cell lines cultured with U−^{13}C glucose or U−^{13}C glutamine. **H** Comparison of the 6 isotopologues in citrate in control, 200 nM rotenone induced OXPHOS dysfunction wit and without pyruvate-uridine treatment; fibroblasts cell lines cultured with U−^{13}C glucose or **I** U−^{13}C glutamine. **J** Pharmacological inhibition of OXPHOS by exposing 7 days old zebrafish larvae to 200 nM rotenone for 6 h**. K** Heartbeat based survival curve comparing the 200 nM rotenone zebrafish model with and without coincubation with 25 mM pyruvate and 25 mM uridine. Mantel−Cox test for curve comparison; > 100 larvae per group. Unless otherwise specified, statistics: one-way ANOVA with post-hoc Dunnett's T3 multiple comparison tests, effect of treatment was assessed using paired student T-tests comparing no treatment with a treatment and the error bars are +/−SD. αKG: alpha-ketoglutarate; dpf: days post fertilisation; Glycerol-3-P: Glycerol-3-phosphate; OXPHOS: oxidative phosphorylation system; PDH: pyruvate dehydrogenase; P + U: pyruvate + uridine.

hypothesized that correcting the metabolic changes could rescue the proliferation defect. To this end, we used the Incucyte® proliferation assay as a screening tool for potential nutritional therapies. This rapid and straightforward assay allowed us to test several nutritional supplementation treatments. The nutrient choice was based on the metabolomics results with the additional requirements that the nutrient had to be a chemically stable and plasma membrane permeable. A first category of therapies was designed to try to restore the depleted metabolites such as citrate, pyruvate, aspartate (provided as the esterified form in order to be able to cross the cell membrane) or to palliate for the hypothesized shortage in nucleotides e.g., uridine (additionally bypassing the mitochondrially located enzyme dihydroorotate dehydrogenase (DHODH)), adenine, guanine, or thymidine. The second category of nutrients was aimed at providing the cells with alternative ways to regenerate NAD+: fructose (by fuelling sorbitol dehydrogenase), pyruvate (using LDH), dehydroascorbic acid (oxidized form of vitamin C) and acetoacetic acid (sustaining hydroxybutyrate dehydrogenase activity). A third strategy was to increase the NAD + pool through supplementation with nicotinamide dinucleotide (NAD) itself or its precursor niacin (vitamin B3). The last strategy aimed to reduce the need for NAD + by inhibiting poly ADP ribose polymerase (PARP), a big consumer of NAD+, by 3-aminobenzamide. We subsequently also applied combinations of different 'successful therapies' to investigate whether synergistic effects could be obtained. Therapies were ranked based on the positive effect on the doubling time (Table S1). The most effective treatments to correct the proliferation deficit were the therapies including pyruvate with or without supplementation with uridine and/or niacin. The addition of the combination pyruvate and uridine to the growth medium induced a significant improvement of the doubling time of the OXPHOS deficient groups (Figure 4B). This successful nutritional intervention was also confirmed by a significant increase in cell counts after 72h ($p = 0.002$; Fig. S2C). No adverse effect on proliferation was observed in the control or the PDH deficient group (Table S1). Because the best results were obtained in the group treated with the combination of pyruvate and uridine, we opted for this combination therapy as potential treatment for OXPHOS dysfunction. Supplementation with uridine alone or the combination of pyruvate with other nucleotides as adenine/guanine or thymidine did not increase the proliferation rate of the fibroblasts (Table S1).

We also applied our therapy on the pharmacologically triggered OXPHOS dysfunction with rotenone, antimycin A or azide and we found, similarly to the genetically affected cell lines, a complete correction of the doubling time and cell counts after 72 h bringing them back into the normal range (Figure 5B, Fig. S2F).

3.8. Supplementation with pyruvate and uridine corrects the metabolic profile in OXPHOS deficiency

To evaluate whether the combination treatment restores the metabolic changes characterizing cells with OXPHOS dysfunction, described above, we performed the previously described tracer metabolomics experiments on a set of 8 control cell lines, 9 cell lines with OXPHOS deficiency (5 CI deficiency; 2 CIV deficiency and 2 combined deficiency) and 2 cell lines with PDH deficiency using fully labelled glucose (U−^{13}C glucose) and glutamine (U−^{13}C glutamine) in the presence of pyruvate and uridine. In addition, we also decided to investigate the positive effect triggered by pyruvate using labelled pyruvate (U−^{13}C pyruvate) tracing. Oxygraphy testing confirmed that this pyruvate-uridine combination did not correct the underlying OXPHOS defect (Fig. S4).

Whereas the treatment did induce a rise in abundance of glycolytic and TCA intermediates as well as nucleotides in all groups, the importance of the improvements was most significant in the OXPHOS dysfunction group (Figure 4E−F). Our results indeed pointed towards a complete restoration of metabolic activities in the OXPHOS deficient group upon treatment with pyruvate and uridine in terms of abundances and fractional contribution (Figure 4C). In OXPHOS dysfunction, we noticed a decrease of the lactate/pyruvate ratio into normal ranges (from 1.8-fold increase to 1.2-fold increase of the ratio in untreated controls; treatment effect $p = 0.04$; Fig. S2G) as well as a normalisation of the TCA cycle intermediates and of aspartic acid levels (Figure 4D−E). In addition, the glycerol-3-P levels decreased back into the control ranges (Figure 4F). We further found that the treatment increased the entry of glucose carbons into the TCA cycle, with an observed normalisation of the m2 labelling from U−^{13}C glucose in citric acid (Figure 4H). A return to oxidative cycling of glutamine in the TCA as illustrated by higher m4 isotopologue of citric acid in OXPHOS dysfunction was also measured. In controls, the glutamine anaplerosis remained unchanged (Figure 4I). The change in the oxidative/reductive cycling of glutamine derived carbons could be linked to a lowered aKG/citrate ratio [22]. Indeed, in OXPHOS deficiency this relative ratio dropped from approximately 2.5 to 1 upon treatment (treatment effect $p = 0.003$; Fig. S2H). A detailed overview of the treatment effect on the relative abundances of aspartate, proline, lactate and glycerol-3P per OXPHOS deficient cell line is provided in Figs. S3A−H.

The tracer data from U−^{13}C pyruvate showed that pyruvate is mainly directed towards lactate, alanine and the TCA cycle (Figure 4C). The conversion of pyruvate into lactate via LDH is a way for the OXPHOS deficient cells to restore the NAD^+/NADH balance through the regeneration of NAD^+. The importance of the LDH mediated reduction of pyruvate in the treatment mechanism is highlighted by the absence of an effect on the proliferation upon pyruvate and uridine treatment when LDH was inhibited by NHI-2 [24] (Fig. S2D).

The conversion of pyruvate into alanine via the alanine transaminase further supports the TCA anaplerosis of glutamine derived carbons. Finally, entry of pyruvate derived carbons via PDH (evidenced by the m2 isotopologue of citric acid) was also observed (Figure 4C).

We also applied our pyruvate + uridine combination therapy on the rotenone triggered dysfunction and found a similar rescue. Pyruvate and uridine replenished the pools of the depleted metabolites, lowered the abundance of glycerol-3-P and corrected the glucose and glutamine carbon entry into the TCA cycle (Figure 5C−F). Moreover, this treatment was also able to relieve the mitochondrial membrane hyperpolarisation caused by chronic rotenone, antimycin A or azide treatment (Fig. S2E).

The effect of treatment in PDH deficiency was non-conclusive in the 2 tested cell lines.

3.9. Pyruvate and uridine increase survival of zebrafish exposed to rotenone

Finally, we tested the efficacy of the treatment with pyruvate and uridine in an *in vivo* model of PMD. We exposed 7 days old zebrafish larvae to rotenone and investigated whether our treatment could rescue the rotenone induced phenotype (Figure 5J). Pharmacological models of PMD in zebrafish have already been validated to investigate disease mechanisms and test potential treatments [13,16]. A titration of rotenone concentration in the zebrafish water revealed a deleterious effect starting from 150 nM. At 200 nM and 150 nM of rotenone, the larvae died quickly with 13.5% and 60% mean survival at 4 h respectively (Figure 5K and Fig. S5). When treated simultaneously with high doses of pyruvate and uridine (25 mM each), this survival increased to 44% and 80% at 4 h in the 200 nM and 150 nM rotenone

groups respectively ($p < 0.0001$; Mantel—Cox test for curve comparison with >80 larvae per group).

4. DISCUSSION

Diagnosis and treatment of PMD remain an actual and unmet medical need [6,9,25]. Not only are those disorders challenging to diagnose even in the genomics era, but they also lack effective treatments in the majority of cases. Therefore, understanding the metabolic consequences of OXPHOS dysfunction at the cellular level could help navigating the clinical heterogenicity, assist the interpretation of genomics data, and provide new insights for therapeutic interventions. In our study, we aimed to understand the underlying metabolic changes by applying tracer metabolomics on validated model systems of disrupted OXPHOS. By tracing the carbon flow of the nutrients glucose and glutamine in cells derived from patients with different genetically defined causes of PMD, we identified several key metabolic changes supporting the major importance of an NAD+/NADH imbalance in PMD. Whereas this imbalance is not novel in the field of PMD, it does highlight the need to investigate the consequences of this imbalance and search for new therapies to restore that balance [7,8,26].

We present here the discovery of a new intracellular marker associated with OXPHOS deficiency: the depletion of aspartic acid. While aspartic acid depletion upon mitochondrial dysfunction and its consequence on proliferation have been reported in the field of cancer research, it is a novel and interesting insight in the field of PMD, especially regarding the actual diagnostic challenge [19,20,27]. Up to now, diagnostic tools for suspected mitochondrial disease include the quantification of plasma amino acids. Plasma aspartic acid levels are low in humans and do not reflect intracellular levels because most cells lack a plasma membrane transporter for aspartate [27—29]. Based on our results, investigating whether e.g., blood cells from patients with PMD also exhibit diminished intracellular aspartic acid could constitute a rapid and easy test to identify OXPHOS dysfunction in patients. This application could fill a need and be useful outside the field of inborn errors of metabolism (IEM) such as for the identification of patients with secondary mitochondrial dysfunction, and/or guide evaluations of potential therapy as a clinical trial surrogate endpoint.

In this study, we applied several treatment strategies for OXPHOS dysfunction aiming at correcting the proliferation deficit that was previously observed. In our disease models, few therapies triggered an improved proliferation of the OXPHOS deficient fibroblasts. Nevertheless, we identified a potential nutritional therapy for OXPHOS dysfunction, i.e., the combination of pyruvate and uridine. This was validated and shown to be very effective in correcting the proliferation deficit of OXPHOS deficient fibroblasts and the observed metabolic profiles thereof. Moreover, the therapy was applied successfully in an *in vivo* zebrafish disease model in which addition of pyruvate and uridine clearly increased the survival rate of zebrafish larvae exposed to lethal concentrations of rotenone. While pyruvate and uridine are traditionally supplemented in the growth medium of cells with mitochondrial dysfunction [30,31], it has, to our knowledge, not been used as a combination therapy for PMD. This also implies that the selection of medium composition for *in vitro* experiments is critical for studying a certain disease. It has recently been reported that this combination therapy was effective in protecting T-cell proliferation from mitochondrial toxicity caused by antibiotics [32]. Pyruvate supplementation on its own has been tried out in several patients suffering from mitochondrial diseases [33—38]. The authors reported positive effect on biochemical parameters and for some patients on clinical outcome such as development, diabetes management, motor function and/or epilepsy. However, a recent meta-analysis concluded on very low evidence for pyruvate supplementation in PMD and recommended additional research on the potential treatment mechanisms and well-designed clinical trials to investigate treatment efficacy [39]. We believe our findings further unravel the faith of supplemented pyruvate and support the need for clinical trials with pyruvate and uridine supplementation in PMD, especially because this treatment offers several advantages. First, it could be administered orally [32—39]. Second, the cost would be low, especially in comparison with targeted therapies including gene editing methods [40]. Last, few side effects of the combination pyruvate and uridine are to be expected [32,39,41]. Doses of 0,5 -1 mg/kg/d pyruvate daily have been described with overall only minor gastro-intestinal side-effects [39]. High doses of uridine triacetate (6.2 g/m2 per os every 6 h) are approved for fluorouracil or capecitabine overdoses with only reports of gastro-intestinal side-effects [41]. We would recommend spreading the intake of pyruvate and uridine as much as possible through the day in order to provide a constant influx into the targeted metabolic pathways. The potential increase of the lactic acidosis of patients with PMD upon pyruvate treatment should be closely monitored during therapy.

Contrasting with previously published reports and studies, the administration of NAD-precursors was not successful [7,26,42]. This lack of effect could stem from the dosages and frequency of administration used in our assay, or from the rapid decay of NAD precursors *in vitro.* Despite positive reports [26], the absence of positive effect of reduction of NAD^+-use following PARP-inhibition was not surprising knowing the implications of PARP- enzymes in key processes such as cell cycle regulation and their use as anti-proliferating agents in cancer medicine [43—45]. Previous reports had shown an improved proliferation upon supplementation with aspartic acid (or its cell-membrane permeable, esterified form) [19,20,26]. We could not confirm these findings in our tested models. We can, however, not exclude that, we may have missed more discrete beneficial effects of some of the tested treatment strategies since many factors play a role in the cell cycle regulation and thus proliferation [46,47]. We can also not exclude that the intracellular delivery of the nutrients, the chosen dosages or the possible metabolization in our disease model (fibroblasts) was not optimal and that those therapies might have a positive effect on other symptoms or in other disease models [48].

This study illustrates the relevance of using tracer metabolomics to identify disease pathophysiology and design therapeutic interventions in the field of IEM [49]. Tracer metabolomics first provided novel insights in the pathomechanisms of PMD which subsequently led to the design of a new nutritional treatment for OXPHOS dysfunction. The choice of the therapy was based on a thorough evaluation of the tracer metabolomics results and aimed at targeting critical aspects of the identified metabolic changes or adaptations. Broader insight in the rewired cellular metabolism as a whole, beyond the pathway affected primarily by the causative enzyme defect, shows great potential for the understanding of phenotypical aspects of IEMs, caused by more distant metabolic adaptations, and can inspire novel therapeutical approaches.

AUTHORSHIP CONTRIBUTION STATEMENT

Isabelle Adant: Conceptualization, Data curation, Formal analysis, Investigation, Methodology, Validation, Visualization and Writing - original draft. Matthew Bird: Conceptualization, data curation, funding acquisition, Project administration, Methodology, Supervision, Visualization, Writing - review & editing. Bram Decru, Marie Wallays, Petra Windmolders: Investigations. Peter de Witte: Resources, Supervision,

Writing - review & editing. Daisy Rymen, Peter Witters: Conceptualization, Supervision, Writing - review & editing. Pieter Vermeersch, David Cassiman, Bart Ghesquière: Conceptualization, Funding acquisition, Methodology, Project administration, Resources, Supervision, Writing - review & editing.

ACKNOWLEDGEMENTS

Funding: This work was supported by the Katholieke Universiteit Leuven (C1 grant: EFF-D2860-C14/17/110) (DC, BG, PV) and the Tjallingh Roorda Foundation (IA). PV and PW are senior clinical investigators of the Research Foundation Flanders (1842020N, T001116N).
We thank Johan Van Hove (Children's Hospital Colorado) for the kind contribution of cells and Jan Maes (Molecular Biodiscovery lab, KUL) for the technical guidance on the zebrafish experiments. We also thank all patients who agreed to participate in this study.

CONFLICT OF INTEREST

None declared.

APPENDIX A. SUPPLEMENTARY DATA

Supplementary data to this article can be found online at https://doi.org/10.1016/j.molmet.2022.101537.

REFERENCES

[1] Gorman, G.S., Chinnery, P.F., DiMauro, S., Hirano, M., Koga, Y., McFarland, R., et al., 2016. Mitochondrial diseases. Nature Reviews Disease Primers 2:1—23.
[2] Sanderson, S., Green, A., Preece, M.A., Burton, H., 2006. The incidence of inherited metabolic disorders in the West Midlands, UK. Archives of Disease in Childhood 91:896—899.
[3] Grier, J., Hirano, M., Karaa, A., Shepard, E., Thompson, J.L.P., 2018. Diagnostic odyssey of patients with mitochondrial disease Results of a survey. Neurol Genet 4, 0—6.
[4] Distelmaier, F., Koopman, W.J.H., Van Den Heuvel, L.P., Rodenburg, R.J., Mayatepek, E., Willems, P.H.G.M., et al., 2009. Mitochondrial complex I deficiency: from organelle dysfunction to clinical disease. Brain 132:833—842.
[5] Hirst, J., 2013. Mitochondrial complex i. Annual Review of Biochemistry 82: 551—575.
[6] Chinnery, P.F., 2015. Mitochondrial disease in adults : what ' s old and what ' s new. EMBO Molecular Medicine 7:1503—1512.
[7] Lee, C.F., Caudal, A., Abell, L., Nagana Gowda, G.A., Tian, R., 2019. Targeting NAD + metabolism as interventions for mitochondrial disease. Scientific Reports 9:1—10.
[8] Esterhuizen, K., van der Westhuizen, F.H., Louw, R., 2017. Metabolomics of mitochondrial disease. Mitochondrion 35:97—110.
[9] El-hattab, A.W., Zarante, A.M., Almannai, M., Disorders, M., Hospital, T., Emirates, U.A., et al., 2018. Therapies for mitochondrial diseases and current clinical trials. Molecular Genetics and Metabolism 122:1—9.
[10] Mathew, A.K., Padmanaban, V.C., 2013. Metabolomics: the apogee of the omics trilogy. International Journal of Pharmacy and Pharmaceutical Sciences 5:45—48.
[11] Bird, M.J., Adant, I., Windmolders, P., Elst, I.V., Felgueira, C., Altassan, R., et al., 2019. Oxygraphy versus enzymology for the biochemical diagnosis of primary mitochondrial disease. Metabolites 9.
[12] Distelmaier, F., Valsecchi, F., Liemburg-Apers, D.C., Lebiedzinska, M., Rodenburg, R.J., Heil, S., et al., 2015. Mitochondrial dysfunction in primary human fibroblasts triggers an adaptive cell survival program that requires AMPK-α. Biochimica et Biophysica Acta, Molecular Basis of Disease 1852: 529—540.
[13] Byrnes, J., Ganetzky, R., Lightfoot, R., Tzeng, M., Nakamaru-Ogiso, E., Seiler, C., et al., 2018. Pharmacologic modeling of primary mitochondrial respiratory chain dysfunction in zebrafish. Neurochemistry International 117:23—34.
[14] Ye, F., Hoppel, C.L., 2013. Measuring oxidative phosphorylation in human skin fibroblasts. Analytical Biochemistry 437:52—58.
[15] Prentzell, M.T., Rehbein, U., Cadena Sandoval, M., De Meulemeester, A.S., Baumeister, R., Brohée, L., et al., 2021. G3BPs tether the TSC complex to lysosomes and suppress mTORC1 signaling. Cell 184:655—674 e27.
[16] Pinho, B.R., Santos, M.M., Fonseca-Silva, A., Valentão, P., Andrade, P.B., Oliveira, J.M.A., 2013. How mitochondrial dysfunction affects zebrafish development and cardiovascular function: an in vivo model for testing mitochondria-targeted drugs. British Journal of Pharmacology 169:1072—1090.
[17] Xiao, W., Wang, R.S., Handy, D.E., Loscalzo, J., 2018. NAD(H) and NADP(H) redox couples and cellular energy metabolism. Antioxidants and Redox Signaling 28:251—272.
[18] Gaude, E., Schmidt, C., Gammage, P.A., Dugourd, A., Blacker, T., Chew, S.P., et al., 2018. NADH shuttling couples cytosolic reductive carboxylation of glutamine with glycolysis in cells with mitochondrial dysfunction. Molecular Cell 69:648—663 e7.
[19] Sullivan, L.B., Gui, D.Y., Hosios, A.M., Bush, L.N., Freinkman, E., Vander Heiden, M.G., 2015. Supporting aspartate biosynthesis is an essential function of respiration in proliferating cells. Cell 162:552—563.
[20] Birsoy, K., Wang, T., Chen, W., Freinkman, E., Abu-Remaileh, M., Sabatini, D.M., 2015. An essential role of the mitochondrial electron transport chain in cell proliferation is to enable aspartate synthesis. Cell 162:540—551.
[21] Jha, M.K., Lee, I.K., Suk, K., 2016. Metabolic reprogramming by the pyruvate dehydrogenase kinase-lactic acid axis: linking metabolism and diverse neuropathophysiologies. Neuroscience & Biobehavioral Reviews 68:1—19.
[22] Fendt, S.-M., Bell, E.L.B., Keibler, M.A., Olenchock, B., Mayers, J.R., Wasylenko, T.M., et al., 2013. Reductive glutamine metabolism is a function of the α- ketoglutarate to citrate ratio in cells. Nature Communications 4:2236.
[23] Berger, U.V., Hediger, M.A., 2006. Distribution of the glutamate transporters GLT-1 (SLC1A2) and GLAST (SLC1A3) in peripheral organs. Anatomy and Embryology 211:595—606.
[24] Granchi, C., Roy, S., Giacomelli, C., MacChia, M., Tuccinardi, T., Martinelli, A., et al., 2011. Discovery of N-hydroxyindole-based inhibitors of human lactate dehydrogenase isoform A (LDH-A) as starvation agents against cancer cells. Journal of Medicinal Chemistry 54:1599—1612.
[25] Witters, P., Saada, A., Honzik, T., Tesarova, M., Kleinle, S., Horvath, R., et al., 2018. Revisiting mitochondrial diagnostic criteria in the new era of genomics. Genetics in Medicine 20:444—451.
[26] Gui, D.Y., Sullivan, L.B., Luengo, A., Hosios, A.M., Bush, L.N., Gitego, N., et al., 2016. Environment dictates dependence on mitochondrial complex I for NAD+ and aspartate production and determines cancer cell sensitivity to metformin. Cell Metabolism 24:716—727.
[27] Garcia-Bermudez, J., Baudrier, L., La, K., Zhu, X.G., Fidelin, J., Sviderskiy, V.O., et al., 2018. Aspartate is a limiting metabolite for cancer cell proliferation under hypoxia and in tumours. Nature Cell Biology 20:775—781.
[28] Sharma, R., Reinstadler, B., Engelstad, K., Skinner, O.S., Stackowitz, E., Haller, R.G., et al., 2021. Circulating markers of NADH-reductive stress correlate with mitochondrial disease severity. Journal of Clinical Investigation 131:1—16.
[29] Clarke, C., Xiao, R., Place, E., Zhang, Z., Sondheimer, N., Bennett, M., et al., 2013. Mitochondrial respiratory chain disease discrimination by retrospective cohort analysis of blood metabolites. Molecular Genetics and Metabolism 110: 1—18.
[30] King, M.P., Attardi, G., 1989. Human cells lacking mtDNA: repopulation with exogenous mitochondria by complementation. Science 246:500—503, 80.

[31] Bodnar, A.G., Cooper, J.M., Leonard, J.V., Schapira, H.V., 1995. Respiratory-deficient human fibroblasts exhibiting defective mitochondrial DNA replication. Biochemical Journal 305:817—822.

[32] Battaglia, S., De Santis, S., Rutigliano, M., Sallustio, F., Picerno, A., Frassanito, M.A., et al., 2021. Uridine and pyruvate protect T cells' proliferative capacity from mitochondrial toxic antibiotics: a clinical pilot study. Scientific Reports 11:1—9.

[33] Komaki, H., Nishigaki, Y., Fuku, N., Hosoya, H., Murayama, K., Ohtake, A., et al., 2010. Pyruvate therapy for Leigh syndrome due to cytochrome c oxidase deficiency. Biochimica et Biophysica Acta (BBA) - General Subjects 1800: 313—315.

[34] Koga, Y., Povalko, N., Inoue, E., Nashiki, K., Tanaka, M., 2019. Biomarkers and clinical rating scales for sodium pyruvate therapy in patients with mitochondrial disease. Mitochondrion 48:11—15.

[35] Koga, Y., Povalko, N., Katayama, K., Kakimoto, N., Matsuishi, T., Naito, E., et al., 2012. Beneficial effect of pyruvate therapy on Leigh syndrome due to a novel mutation in PDH E1α gene. Brain & Development 34:87—91.

[36] Fujii, T., Nozaki, F., Saito, K., Hayashi, A., Nishigaki, Y., Murayama, K., et al., 2014. Efficacy of pyruvate therapy in patients with mitochondrial disease: a semi-quantitative clinical evaluation study. Molecular Genetics and Metabolism 112:133—138.

[37] Saito, K., Kimura, N., Oda, N., Shimomura, H., Kumada, T., Miyajima, T., et al., 2012. Pyruvate therapy for mitochondrial DNA depletion syndrome. Biochimica et Biophysica Acta (BBA) - General Subjects 1820:632—636.

[38] Inoue, T., Murakami, N., Ayabe, T., Oto, Y., Nishino, I., Goto, Y.I., et al., 2016. Pyruvate improved insulin secretion status in a mitochondrial diabetes mellitus patient. Journal of Clinical Endocrinology and Metabolism 101:1924—1926.

[39] Li, M., Zhou, S., Chen, C., Ma, L., Luo, D., Tian, X., et al., 2020. Therapeutic potential of pyruvate therapy for patients with mitochondrial diseases: a systematic review. Ther Adv Endocrinol Metab 11:1—13.

[40] Shukla, V., Seoane-Vazquez, E., Fawaz, S., Brown, L., Rodriguez-Monguio, R., 2019. The landscape of cellular and gene therapy products: authorization, discontinuations, and cost. Hum Gene Ther Clin Dev 30:102—113.

[41] Ison, G., Beaver, J.A., McGuinn, W.D., Palmby, T.R., Dinin, J., Charlab, R., et al., 2016. FDA approval: uridine triacetate for the treatment of patients following fluorouracil or capecitabine overdose or exhibiting early-onset severe toxicities following administration of these drugs. Clinical Cancer Research 22: 4545—4549.

[42] Pirinen, E., Auranen, M., Khan, N.A., Brilhante, V., Urho, N., Pessia, A., et al., 2020. Niacin cures systemic NAD+ deficiency and improves muscle performance in adult-onset mitochondrial myopathy. Cell Metabolism 31:1078—1090.e5.

[43] Perl, A., Menzies, K., Auwerx, J., Physiology, S., 2016. NAD+ metabolism and the control of energy homeostasis - a balancing act between mitochondria and the nucleus. Cell Metabolism 22:31—53.

[44] Genta, S., Martorana, F., Stathis, A., Colombo, I., 2021. Targeting the DNA damage response: PARP inhibitors and new perspectives in the landscape of cancer treatment. Critical Reviews in Oncology 168:103539.

[45] Mateo, J., Lord, C.J., Serra, V., Tutt, A., Balmaña, J., Castroviejo-Bermejo, M., et al., 2019. A decade of clinical development of PARP inhibitors in perspective. Annals of Oncology 30:1437—1447.

[46] Vander Heiden, M., Cantley, L., Thompson, C., 2009. The metabolic requirements of cell proliferation. Science 324:1029—1033, 80.

[47] Zhu, J., Thompson, C., 2019. Metabolic regulation of cell growth and proliferation. Nature Reviews Molecular Cell Biology 20:436—450.

[48] Brumskill, S., Barrera, L.N., Calcraft, P., Phillips, C., Costello, E., 2021. Inclusion of cancer-associated fibroblasts in drug screening assays to evaluate pancreatic cancer resistance to therapeutic drugs. Journal of Physiology & Biochemistry.

[49] Radenkovic, S., Bird, M.J., Emmerzaal, T.L., Wong, S.Y., Felgueira, C., Stiers, K.M., et al., 2019. The metabolic map into the pathomechanism and treatment of PGM1-CDG. The American Journal of Human Genetics 104: 835—846.

